

Leveraging Persistent Homology Features for Accurate Defect Formation Energy Predictions via Graph Neural Networks

Zhenyao Fang* and Qimin Yan*

Department of Physics, Northeastern University, Boston

E-mail: z.fang@northeastern.edu; q.yan@northeastern.edu

Abstract

Accurate predictions of defect formation energies are crucial to understanding defect properties in materials, such as favorable defect types and concentration, and to investigating the interplay between defects and other functional properties of materials. To overcome the computational expense of density-functional theory calculations in large supercells, several graph neural network (GNN) models were proposed to predict the defect formation energies. However, their performance is limited due to the fact that defect formation energies depend strongly on the local atomic configurations near the defect sites and to the over-smoothing problem of GNN. Herein, we demonstrate that persistent homology features, which characterize the topological structure of the local chemical environment around each atomic site, encode the structural information of defects (such as vacancies and substitutions), including the size of the defects, the number of defects near each atom, and the distance to those defects. Using the dataset comprising a wide spectrum of O-based perovskites with vacancies of various elemental type as an example, we construct and train the GNN models to predict the neutral

vacancy formation energies, and show that incorporating the persistent homology features, along with proper choices of the graph pooling operations, significantly increases the prediction accuracy and overcomes the non-convergence issue with respect to the supercell size in previous GNN models. Furthermore, using defective BaTiO₃ with multiple substitutions and multiple vacancies as examples, our GNN model can also predict the defect-defect interaction energies in materials accurately. These results suggest that persistent homology features are highly effective in predicting defect-related properties and can be integrated into the vast family of advanced graph neural network models for future defect studies.

Introduction

Understanding the effect of point defects in materials has been a central area of study in materials science as defects can significantly alter the physical and chemical properties of materials, such as reducing the bulk modulus and inducing structural phase transitions,¹⁻³ and introducing in-gap defect states which can further affect their performance in optoelectronic devices and catalysts.⁴⁻⁶ One of the key quantities in defect chemistry is the defect formation energy,^{7,8} from which various defect properties can be directly determined, such as the favorable type of defects and the location of defects in a given host material, the defect concentration at certain temperature, and defect migration pathways near surfaces or grain boundaries.^{9,10} Therefore, fast and accurate predictions of defect formation energies are crucial to understanding various defect-related phenomenon in materials, enabling high-throughput screening of host material with desired defect properties and future studies on the interplay between defects and disorder.

To evaluate the defect formation energies, first-principles calculations based on density functional theory (DFT) are often employed.^{8,11,12} However, this method often involves large supercell calculations that are computationally expensive in order to achieve the dilute defect limit. Therefore, various machine learning methods along with physics-inspired descriptors

(such as the formation enthalpy, the energy above hull, the band gap, and the crystal reduction potential) were proposed to accelerate calculating defect formation energies.¹³⁻¹⁷ Although these machine learning models have achieved great accuracy in predicting defect formation energies, they lack the generality to accommodate a wide spectrum of materials, as they depend on human-selected features that are effective on specific types of materials. Besides, due to the model architecture, most proposed machine learning models cannot evaluate the formation energies for different symmetry-inequivalent atomic sites, restricting their applications in predicting defect formation energies in complex materials that can potentially host multiple defects.

Recent years, graph neural networks (GNNs) have shown remarkable success in predicting various material properties, including the formation enthalpy, band gap, and bulk modulus.¹⁸⁻²⁰ In a GNN model, the input crystal structure will be converted into a graph, where the nodes and edges represent the atoms and bonds in the unit cell.²¹ The graph will be then passed through several convolution layers, where node information will exchange between adjacent nodes and aggregate together, allowing the GNN model to learn the local chemical environment of each atom and to extract latent representations of the whole crystal, which will be used to make predictions on material properties. However, few GNN models have been applied to predict defect formation energies.²²⁻²⁴ As first attempts to apply GNNs to predict defect related properties, these models incorporated various levels of chemical information, including the bond angle which may help detect the disrupted chemical bonding network near the vacancies,²⁴ but their prediction accuracy is currently limited. The reasons for the poor performance of GNNs on predicting defect formation energies are two-fold. Firstly, defect formation energies highly depend on the atomic configurations near the defective sites and are independent of the atoms far from the defective sites, and are thus local properties of the crystal, contrary to the formation enthalpy or the band gap that are global quantities of the whole crystal structure. Secondly, GNNs suffer from the over-smoothing problem.²⁵ When passing through consecutive convolution layers, the fea-

tures between adjacent nodes will exchange and aggregate, and finally converge to constant values in a deep GNN model. This could lead to incorrect predictions especially when the prediction target only depends on the local atomic configurations. Therefore, in order for GNNs to accurately predict the defect formation energies, structural information about the defects, such as distances to defective sites or the number of nearby defects of, must be encoded explicitly in the features of each node, so that differences between atoms near or far from the defects are amplified, which can potentially reduce the over-smoothing effect of GNN and direct the attention of the neural network to atomic sites near the defects.

Based on these motivations, we propose to incorporate the persistent homology features into the node features and apply them to attention-based GNN models to predict defect formation energies. Persistent homology features are generated from topological invariants of the homology group associated with the surrounding atomic configurations near each atom.^{26,27} These features have already been applied in topological data analysis and predicting (global) properties of molecules and materials, such as the formation enthalpy.^{28,29} In this work, we demonstrate that persistent homology features entail the local structural information related to defects and can significantly increase the prediction accuracy of defect formation energies in complex materials. We show from several toy models that persistent homology features contain such information as the size of defects, the number of defects around each atom (within a cutoff radius), and the distance to the defects from each atom. To verify the efficacy of persistent homology features, we construct the GNN model based on neural networks with the attention mechanism, and train on the dataset containing around 7700 O-based perovskite defective structures with mono-vacancies. With proper choices of the elemental attributes and the graph pooling layers, we find that the introduction of persistent homology features significantly decreases the mean absolute error (MAE) from 1.55 eV to 0.74 eV, outperforming previously proposed GNN models.^{24,30} Besides, we also apply the GNN model to datasets of cubic perovskite BaTiO₃, a well-known prototypical cubic perovskite,³¹ with multiple substitutions and multiple defects, and we show that the persistent

homology features also help with capturing the defect-defect interaction energies in those datasets. These results suggest the crucial role of persistent homology features in extracting local structural information near defects and in predicting physical and chemical properties related to defects in complex materials.

Results and Discussions

Persistent Homology Features and Defects

Given a simplicial complex X formed by gluing "standard" geometric objects (simplicies) of various dimensions (such as points, line segments, triangles, tetrahedrons) together, its homology property generally refers to its d -Betti number $\beta_d(X)$, defined as the rank of the homology group $H_d(X)$. Any nontrivial element in the homology group $H_d(X)$ corresponds to some d -dimensional cycle (cyclic simplices) that is not simultaneously the boundary of any $(d + 1)$ -dimensional chain, namely a d -dimensional "hole"; for example, a circle is a one-dimensional cycle and encloses a hole, while the boundary of a disk, though also being a one-dimensional cycle, does not enclose a hole since it is the boundary of the two-dimensional disk. Therefore, the d -Betti numbers characterize the number of d -dimensional holes in the simplicial complex and contain the connectivity information of the simplicial complex (see Supplementary Materials I for definitions).³² In the context of topological data analysis, any set of data points can be converted into a simplicial complex by connecting the points together within some cutoff radius, which is allowed to vary so that the underlying pattern behind the given set of data points can be revealed through the birth, the death, and the persistence of Betti numbers (see Supplementary Materials I for more discussions).^{26,33,34}

In chemical systems such as molecules or materials, the atomic configuration can be naturally regarded as a point cloud, and the chemical bonding network as a simplicial complex, allowing for the calculations of persistent homology features. Previous work introduced atom-specific persistent homology (ASPH) features as a topological representation of crystal

structures.²⁹ For each base atom in the unit cell, a point cloud is generated such that it includes all other atoms within the given upper bound cutoff radius from the base atom for each chemical species. The persistent homology features are then calculated for each point cloud; since crystalline materials are three-dimensional, only 0-, 1-, and 2-Betti numbers are relevant. The birth, death, and persistence of these Betti number features are further characterized by five statistical quantities, including the minimum, maximum, mean, standard deviation, and the (weighted) sum, resulting in 35 statistical representations of the persistent homology features for each atom in the unit cell. An example is shown in Fig. 1(A), where the crossed atom represents the vacancy in the two-dimensional lattice. The point cloud centered at the red atom includes the vacancy site while that at the black atom excludes the vacancy site and their calculated persistent homology features are distinct.

Since persistent homology features can detect the number of "holes" within the point cloud near each atom, we conjecture that these features can also unveil the structural changes induced by defects; in this work we examine two of the most common defect types, namely vacancies and substitutions. Vacancies can be regarded as "holes" in a material and thus be detected by persistent homology features, while substitutions, as we will demonstrate below, are also encoded in these ASPH features, since the point cloud is constructed for each chemical species around the base atom.

To verify our hypothesis, we construct a toy model consisting of a one-dimensional atomic chain with equal interatomic spacing (1 \AA), and we create a vacancy in the chain, as shown in Fig. 1(B). Since this is a one-dimensional chain, only 0-Betti numbers are relevant; therefore, we calculate the 0-Betti number features for all atoms with the upper bound cutoff radius to be 3 \AA and generate the statistical quantities of the death of these features. As discussed in Appendix I, 0-Betti numbers reflect the connected components in the simplicial complex. For atoms that are at least 3 \AA far away from the vacancy site, the point cloud around them does not contain the vacancy site. Thus, the maximum of the death of 0-Betti numbers is 1 \AA , above which all atoms in the point cloud are connected with each other, forming

one trivial connected component. On the other hand, for atoms within 3 \AA to the vacancy site, the maximum death of their 0-Betti numbers increases to 2 \AA which is needed for the two connected components to the left and right of the vacancy to connect with each other. Therefore, the 0-Betti number features can help distinguish the atoms close or far from the defect site, separated by the upper bound cutoff radius.

Furthermore, we consider the toy model with two adjacent vacancies, and the calculated features are shown in Fig. 1(C). In this case, we define the position of the vacancy to be the center of the two missing atoms; therefore, the distance of the nearest neighbor to the vacancy site is 1.5 \AA . The maximum of the death of the 0-Betti numbers for atoms close to the vacancy sites increases to 3 \AA , because the cutoff radius must be at least 3 \AA in order to connect all atoms together.

Apart from vacancies, we argue that ASPH features are also sensitive to substitutions. By definition, for each atom in the unit cell, the point cloud which will be used to calculate persistent homology features is constructed for each chemical species. Therefore, when an atom is substituted by an exotic species, the point cloud for this species will contain only two points (connected components), and the critical distance at which these two points are connected is exactly the distance to the substitution site. This is confirmed by the above toy model with one substitution site, whose calculated features are shown in Fig. 1(D).

Finally, in the two-dimensional case, not only the 0-Betti numbers, but also the 1-Betti numbers are relevant. Therefore, we calculate the 1-Betti number properties, shown in Fig. 1(E), for a two-dimensional lattice with one vacancy. In this case, the death of the 1-Betti number indicates the critical cutoff radius at which the hole formed by the vacancy is filled, and is thus different for atoms close and far from the vacancy site. More discussions on the toy models, including two distant vacancy and multiple element cases, can be found in Appendix I. These results demonstrate that persistent homology features can capture the structural information near the vacancies, including the number of vacancies near each atom, the distance to those vacancies, and also the size of the vacancies.

Vacancy Formation Energy in O-Based Perovskites

To numerically verify the capability of persistent homology features in capturing local structural information of defects and improving prediction accuracy of defect-related properties in complex materials, we construct GNN models based on attention mechanism to predict neutral defect formation energies in various datasets according to Eq. 1.

Our GNN model features a typical graph property prediction model architecture, shown in Fig. 2. First, the supercell structure of the defective structure is converted into a graph, where the nodes and the edges of the graph represent the atoms and chemical bonds in the crystal. The node features carry the atomic information of each atom, including the elemental attributes and the ASPH features. In this work, we consider three types of elemental attributes: atomic number (only), elemental properties (including the atomic number, atomic mass, atomic radius, electron affinity, row and group numbers), one-hot encoding of the elemental type.²¹ The complexity and representation capability progressively increases for these three different options, where the atomic number attribute has been used to predict configurational disorder related properties which usually involve few elements while the one-hot encoding attribute was used to predict the formation enthalpy and the band gap of a wide range of materials in Materials Project.³⁵ On the other hand, the edge features represent the bonding properties, which in our case are the bond lengths expanded in a Gaussian function basis. Note that in other types of higher-order GNN models, more information about the atoms and the bonds in crystal, such as the bond direction and the bond angle as well as the multiplet interactions, can also be included in the graph.^{36,37}

The generated graph then passes through several graph convolution layers, where each node receive information from adjacent nodes and aggregate them together; these convolution operations provide each node with their chemical environment information. Depending on the methods to aggregate and update node features, various convolution layers were proposed. In this work, we compare the performance of two types of convolution layers with attention mechanism (the graph attention neural network (GAT)^{38,39} and the Transformer

network⁴⁰) and one without the attention mechanism (the crystal graph neural network (CGNN)²¹). In attention-based neural networks, the information from adjacent nodes is expressed as attention coefficients that are calculated from the node features and edge features and indicate the similarity between the two adjacent node features in the latent space, namely, the similarity in the elemental properties and also persistent homology features in our case. The node features are then updated by a linear combination of all adjacent node features weighted by the attention coefficients. The attention mechanism allows the GNN model to capture the chemical and structural distinctions between adjacent atoms and in general leads to better performance on various tasks. Finally, after the graph convolution layers, all node features in the graph are gathered together through graph pooling layers to obtain the latent representations of the whole crystal, which will be further passed to a multi-perceptron network to obtain the defect formation energy. We will demonstrate below that the choices of node features, graph convolution layers, and pooling layers significantly affect the performance of GNN models, and for the tasks related to predicting defect properties, the optimal choices of the model architecture are different from typical GNN models used to predict the formation enthalpy or band gap.

Now we demonstrate the efficacy of persistent homology features using the dataset containing O-based perovskite defective structures. Here we consider all available monovacancies in these structures. To construct our dataset, we choose all perovskite structures with the chemical formula ABO_3 from materials project,³⁵ excluding those with cations after Ba in the periodic table. On one hand, most elements after Ba (such as the f -block elements, $6p$ and $6d$ elements) require further detailed investigations on the optimal $U(J)$ values that highly depend on individual perovskite structures within the DFT+U framework. On the other hand, excluding structures with those elements in our dataset does not affect the generalizability of our GNN models because their elemental attributes can be easily integrated into the node features. Next we use the pymatgen-analysis-defects package^{41,42} to generate supercells that are necessary to calculate the defect formation energies for each perovskite

structure. The supercells are constructed as nearly cubic cells with the minimal (maximal) lattice constants along each direction being 10 Å (25 Å), so that the interactions between defects and their periodic images along each Cartesian direction are negligible. Structures whose supercells cannot be constructed into the nearly-cubic cell are discarded. After excluding those structures, we obtain around 1100 host perovskite structures. Using the generated supercells, we enumerate all available symmetry-inequivalent atomic sites and generate the corresponding vacancy structures. The total number of defective structures is around 7700, and the number of each type of vacancy is shown in Fig. 3(A). This dataset contains vacancies of all elements (before Ba, and except noble gas elements) and perovskites in all crystal systems, which makes it challenging for GNN models to learn and predict. Some of the most common vacancy types are also listed in Tab. 1.

Table 1: The number of vacancies of the most common elemental types in the constructed O-based perovskite dataset.

vacancy type	O	Sr	Te	Cr	Ca	Fe	V
number	4049	216	203	178	173	171	161

First we present benchmark calculations on our dataset of defective O-based perovskites. Previous GNN models,³⁰ which were based on GAT and Transformer network and only used the elemental attributes as the node features, showed high accuracy in predicting the total energies in configurationally disordered materials. Since our defective perovskite structures typically contain vacancies at various atomic sites, we manually add one fictitious atom to the vacancy site in each defective structure, with its node feature distinct from that of any other elements in the dataset. In this way, those defective structures have the same chemical bonding network as their corresponding host material, but with one randomly chosen element being replaced by the fictitious atom, similar to case of configurational disorder. By training the previously proposed GNN model on the O-based perovskite dataset with fictitious atom, the MAE is found to be 1.77 eV. On the other hand, higher-order GNN models, such as the atomistic line GNN (which also used only the elemental attributes), further incorporated

the bonding angle into the model, allowing the model to capture the disrupted chemical bonding network near the defect sites and make more accurate predictions about defect-related properties.²⁴ However, after training on our dataset, the MAE is 1.86 eV. The poor performance of these models demonstrates the challenge of our constructed dataset, but more importantly, the uniqueness of defect-related property prediction tasks. Firstly, huge supercells are usually required in defect calculations in order to reach the dilute defect limit. Since GNN models will perform graph pooling operations on all node and gather all node features together as the global representation of the graph, the distinct node features of atoms near the defect site, generated either by the presence of nearby fictitious atom (representing the vacancy) or by a disrupted chemical bonding network (as is the case in atomistic line GNN), are averaged out by the node features of the numerous atoms located far from the defects in the supercell. This trend was also present in previous reports,²⁴ where the performance of GNN models generally worsens using larger supercells for defect calculations. Secondly, GNN models suffer from the over-smoothing problems.²⁵ Since the node features are exchanged between adjacent nodes for each convolution layer, the node features will exponentially converge to constant values in a deep GNN model as the number of convolution layers increases. In our scenario, this problem will also average out the node features and make the distinct features carried but atoms near the defect site invisible to the model. Therefore, we choose to explicitly include the local chemical environment information, represented as the persistent homology features that entail the structural changes due to defects, into the GNN model to amplify the differences in node features between atoms located close and far from the defect sites. Along with proper choices of graph pooling layers, the distinct features due to defects are not averaged out by other atoms that do not contribute to the defect properties or by the over-smoothing effect of GNN models.

For each defective structure, we generate the ASPH features (35 statistical quantities of the birth/death/persistence of Betti numbers) for each atom in the supercell. When generating the features, the upper bound cutoff radius can affect the final performance of

the GNN model. With larger upper bound cutoff radius, structural information from farther defects can be included, but computations will also become more expensive. Therefore, we show convergence test results on the cutoff radius in Supplementary Materials II, and determined to use 10 Å as the upper bound cutoff radius to generate the persistent homology features, similar to the typical polaron size of around 8 Å in O-based perovskites.^{43,44} Besides, some of the generated features are correlated with each other. To remove the redundant features, we pre-process the calculated features by principal component analysis method, which reduces the dimensionality of features through linear transformations and concentrates the information in features into the principal components.⁴⁵ As shown in Supplementary Materials II, the MAE reduces as more principal components are included into the node features and reaches convergence above 6 principal components, the sum of the explained variance percentage of which is 99.5%, suggesting that those principal components already contain most of the information from the original 35 persistent homology features in our dataset.

Next we discuss the effect of graph pooling layers. Previous GNN models for material property predictions usually use global mean (sum) pooling layers to all node features together, which calculates the mean (sum) of those features as the global representation of the graph. However, this method includes the contributions from all node features, even for those that are far from the defect sites, and thus average out the distinct features related to defects, as discussed above. Therefore, we choose to use global max pooling layers to extract the maximal features over all nodes, which will direct the attention of our GNN models to distinct features near the defect sites. The MAE using different types of elemental features without and with persistent homology features are summarized in Tab. 2 (the results for other types of pooling layers, such as global sum pooling, global min-max pooling can be found in Supplementary Materials II), and the comparison in the defect formation energy between DFT and GNN (using one-hot encoding with persistent homology features) is shown in Fig. 3(B). We notice that the introduction of ASPH features significantly increases the

prediction accuracy, with the MAE (using the one-hot encoding elemental attributes) reduced by half from 1.55 eV to 0.74 eV. This result demonstrates the crucial role of persistent homology features in capturing the defect structural information and in defect-related property predictions. Besides, the one-hot encoding of the elemental type as the node features lead to better predictions of defect formation energies than the other two types of elemental attributes. Since our dataset contains diverse perovskite structures and a wide range of chemical elements, the atomic numbers or other elemental properties are not sufficient to help distinguish the elements and to make accurate predictions on the dataset, as discussed above. Furthermore, by comparing the performance of our GNN model using one-hot encoding as the elemental attributes but without the persistent homology features (1.55 eV) with our two benchmark calculations using fictitious atom dataset (1.77 eV) and atomistic line GNN (1.86 eV) above, which also used the one-hot encoding as the elemental attributes but global mean (sum) pooling layers, our choice of the global max pooling layer slightly increases the prediction accuracy, consistent with our above conjecture.

Table 2: The comparison of MAE of our constructed GNN models on the O-based perovskite dataset without and with persistent homology features. The elemental attributes are represented as (only) atomic number, or the elemental properties (including the atomic number, atomic mass, atomic radius, electron affinity, row and group numbers), or the one-hot encoding of the elemental type.²¹

	atomic number	elemental properties	one-hot encoding
without	2.02	1.83	1.55
with	1.39	1.25	0.74

As discussed above, one typical problem of GNN models on defect property predictions is the averaging effect from atoms that do not contribute to the defect properties, manifested as the non-convergence of the MAE as the size of the defective supercell increases.²⁴ Here, we demonstrate that the performance of our GNN model which uses global max pooling layers has reached convergence on the supercell size. Since the crystal systems of our host (pristine) perovskites are diverse and the defective supercells are constructed nearly cubic, making it difficult to change the periodicity, we focus on host perovskites only in the cubic

and the tetragonal crystal system, whose transformation matrix to the defective supercell is diagonal. Based on the constructed defective supercells (which already contain hundreds of atoms), we consecutively increase its periodicity in the direction along which the lattice constants are the smallest, assuming that the defect formation energies from DFT methods remain constant (the benchmark results can be found in Supplementary Materials II). We shown the MAE of the trained GNN model on those datasets in Supplementary Materials II. Though the MAE is larger than that trained on the whole dataset, which is possibly due to less amount of data, the MAE is converged with respect to the size of supercells, demonstrating that our GNN model can also adapt the dilute defect limit.

Furthermore, we discuss other types of pooling layers which may also help avoid the over-smoothing problem. In defective structures with mono-vacancies, the distance between each atom and the vacancy site is well-defined. Therefore, we calculate the global representation of the graph by a linear combination of all node features weighted by an exponentially decaying function of the distance whose parameters are learned by the model; atoms farther away from the vacancy site contributes less to the global feature. An alternative option is to pass the distance to a deep multi-perceptron network with limited number of hidden channels which can approximate the highly nonlinear exponential function. The global representation is calculated as the linear combination of all node features weighted by the output of this multi-perceptron network. The MAE of the GNN model in these two cases are 0.82 eV and 0.75 eV respectively, similar to the above results using global max pooling layers, suggesting the strong dependence of defect properties on atomic features near the defect site.

Finally, we narrow our dataset down to structures with only O-vacancies. For the whole dataset, the accurate prediction of the vacancy formation energies requires information about the local chemical environment around the vacancy as well as the elemental type of the vacancy. As we focus on only O-vacancies, the prediction task is simpler than that on the whole dataset since the elemental type information is no longer needed. However, most of the host materials in our dataset still possess multiple symmetry-inequivalent O-sites with

varying vacancy formation energies, making it challenging for previously proposed machine learning and GNN models to tackle. With our GNN model with ASPH features and global max pooling layers, the MAE is 0.45 eV (the comparison between DFT and GNN predictions is shown in Fig. 3(C)), which is comparable to most previous machine learning and deep learning models predicting oxygen vacancy formation energies in oxides.^{46–48}

Multi-Defect Interaction Energy in BaTiO₃

As discussed above, persistent homology features not only contain information about vacancies, but also the substitution defects. Therefore, including persistent homology features can also improve the energies of structures with substitutions. Here we use the cubic perovskite BaTiO₃ as an example and consider the defect formation energies of multiple substitutions. We construct the dataset containing 1000 defective BaTiO₃ in a $3 \times 3 \times 3$ supercell, and randomly replace at most 8 Ba (out of 27) atoms by Ca or Sr and at most Ti (out of 27) atoms replaced by Zr. We train our GNN model with one-hot encoding as the elemental attributes and global max pooling layers to this dataset. After including the persistent homology features, the MAE decreases slightly from 0.07 eV to 0.03 eV, and the comparison between defect formation energies of DFT and GNN methods are shown in Fig. 4(a). We notice that substitution defects do not change the overall chemical bonding network of BaTiO₃, but only replace atoms by other chemical species randomly, similar to the configurationally disordered materials. In this case, even without the persistent homology features, our GNN model which is based on the GNN model for the configurationally disordered materials can already capture the elemental swaps and substitutions and make accurate predictions on the formation energies, and adding the persistent homology features only slightly increases the accuracy.

Furthermore, we consider BaTiO₃ with multiple vacancies. The above discussions revealed that persistent homology features can capture the number of vacancies around each atom. Therefore, persistent homology features can also benefit predictions with multiple

vacancies. To verify this conjecture, we construct another dataset containing 1000 defective BaTiO₃ in a $3 \times 3 \times 3$ supercell, and randomly remove (exactly) 1 Ba, 1 Ti, and 3 O atoms. Since we constrained the number of vacancies and the host material, the energy fluctuations of different defect configurations arise from the vacancy-vacancy interactions. Therefore, the prediction target in fact reflects the multi-vacancy interaction energy; however, for consistency, we still call it the defect formation energy and calculate it from Eq. (1). Again we train our GNN model on this dataset, and the MAE decreases from 0.55 eV to 0.43 eV, where the comparison between DFT and GNN formation energies is shown in Fig. 4(b). The worse performance of vacancy defects than the substitution defects is due to the fact that vacancies disrupt the chemical bonding network in materials and affect the exchange of information indirectly through the adjacency matrix in graphs, making it more challenging to capture the vacancy formation energies than substitution formation energies. Besides, by the construction of atom-specific persistent homology features (Fig. 1), those features are naturally more sensitive to the presence of substitutions as exotic chemical species, while vacancies are obliquely encoded in the birth and death of 1-Betti numbers and 2-Betti numbers. We believe more direct encoding of the vacancy information in the persistent homology features could further improve the prediction accuracy of future GNN models.

Conclusions

In this work, we reveal the relationship between persistent homology features, obtained from the topological invariants of the homology group of point clouds, and the defect structures including (mono-, multi-)vacancies and substitutions. Through several toy models, we demonstrate that persistent homology features contain local structural information near each atom, such as about the number of defects, the distance to those defects, and the size of the defects. These persistent homology features can be easily incorporated into the node features in GNN models and improve the performance of GNN models in predicting defect-related

properties.

We numerically verify the role of persistent homology features using the dataset of O-based perovskite materials, which covers a wide spectrum of crystal systems and elemental vacancy types, and construct and train the GNN models on it to predict the neutral vacancy formation energies. We find that including the persistent homology features can significantly increase the prediction accuracy of GNN models with the MAE reduced by half. Furthermore, we demonstrate that persistent homology features can help predict the defect-defect interaction energies, using the defective cubic perovskite BaTiO_3 with multiple substitutions and with multiple vacancies. These results justify the essential role of persistent homology features in the accurate predictions of defect properties, such as defect formation energies and charge transition levels, through GNN and will benefit future investigations on high-throughput screening and design of host materials and defects with desired properties.

Methods

Density-Functional Theory Calculations

First-principles calculations are carried out using Vienna Ab initio Simulation Package^{49,50} with projector augmented wave pseudopotentials.^{51,52} We used the GGA-PBE functional for all calculations.⁵³ The kinetic energy cutoff of the plane-wave basis sets is 550 eV, the energy convergence threshold is 10^{-6} eV. The Γ -kpoint sampling scheme is used for all pristine and defective supercell calculations, and for elemental energy calculations we used the kpoint grid with the density of $0.03 \frac{2\pi}{\text{\AA}}$. We performed the spin-polarized calculations with the $DFT + U$ scheme for $3d$ elements, with the U values taken from materials project.³⁵ The DFT-D3 method was also used to take account of the van der Waals interactions.^{54,55}

In this work we only consider the neutral charge state for all defects, and therefore the defect formation energy for the defect M_C , following the Kröger–Vink notation, is defined

as

$$E^f[M_C] = E[M_C] - E[\text{bulk}] + \sum_i n_i \mu_i \quad (1)$$

where n_i is the difference in the number of elements between the defective and the pristine structures ($n_i > 0$ for removed atoms and $n_i < 0$ for added atoms), and μ_i is the chemical potential of element i , which we assumed to be the energy of the most stable single crystal of this element (except for H, N, O, F, Cl, which we calculate their energies from corresponding gas molecules).^{7,8}

Training GNN Models

To train our GNN model, our dataset is split into the training set, validation set, and testing set according to 60:20:20 ratio. The validation set is used to prevent overfitting on the training set, which usually occurs when the dataset contains few data. The MAE on the validation set is tracked during the training procedure, and we use the model with the minimal MAE on the validation set as our optimal model for testing.

The set of hyperparameters are optimized based on Bayesian optimization method as implemented in Optuna,⁵⁶ which calculates the expected improvement from a new set of hyperparameters using Tree-structured Parzen Estimator method,⁵⁷ and decides whether to accept or decline this set of hyperparameters. The set of hyperparameters used in this work includes the number of convolution layers, the number of hidden channels in each convolution layers, the number of attention heads (used only in GNN models with attention mechanisms), learning rate, weight decay, and batch size. For GNN models using the information of distance between each atom and the vacancy site, we further add the number of layers and the number of hidden channels in the multi-perceptron network as hyperparameters.

The dataset and the codes used in this work are available on Github at https://github.com/qmatyanlab/Defect_GNN.

Acknowledgement

Z.F. thanks helpful advice from Alex Heilman. This work is supported by the National Science Foundation under Grant No. DMR-2314050. This research used resources of the National Energy Research Scientific Computing Center (NERSC), a U.S. Department of Energy Office of Science User Facility located at Lawrence Berkeley National Laboratory.

Supporting Information Available

The following files are available free of charge.

- Leveraging Persistent Homology Features for Accurate Defect Formation Energy Predictions via Graph Neural Networks: Supplementary Materials

References

- (1) Li, C.; Fu, T.; Hu, H.; Peng, X. Mechanical properties and their sensitivity to point defects: (HfNbTaTiZr)C high-entropy carbide. *Phys. Rev. B* **2022**, *105*, 224102.
- (2) Boström, H. L. B.; Kieslich, G. Influence of Metal Defects on the Mechanical Properties of ABX₃ Perovskite-Type Metal-formate Frameworks. *J. Phys. Chem. C* **2021**, *125*, 1467–1471.
- (3) Dastider, A. G.; Rasul, A.; Rahman, E.; Alam, M. K. Effect of vacancy defects on the electronic and mechanical properties of two-dimensional MoSi₂N₄. *RSC Adv.* **2023**, *13*, 5307–5316.
- (4) Pan, X.; Yang, M.-Q.; Fu, X.; Zhang, N.; Xu, Y.-J. Defective TiO₂ with oxygen vacancies: synthesis, properties and photocatalytic applications. *NANOSCALE* **2013**, *5*, 3601–3614.

- (5) Yin, W.-J.; Yang, J.-H.; Kang, J.; Yan, Y.; Wei, S.-H. Halide perovskite materials for solar cells: a theoretical review. *JOURNAL OF MATERIALS CHEMISTRY A* **2015**, *3*, 8926–8942.
- (6) Leem, Y.-C.; Fang, Z.; Lee, Y.-K.; Kim, N.-Y.; Kakekhani, A.; Liu, W.; Cho, S.-P.; Kim, C.; Wang, Y.; Ji, Z.; Patra, A.; Kronik, L.; Rappe, A. M.; Yim, S.-Y.; Agarwal, R. Optically Triggered Emergent Mesostuctures in Monolayer WS₂. *Nano Letters* **2024**, *24*, 5436–5443.
- (7) Van de Walle, C. G.; Neugebauer, J. First-principles calculations for defects and impurities: Applications to III-nitrides. *Journal of Applied Physics* **2004**, *95*, 3851–3879.
- (8) Freysoldt, C.; Grabowski, B.; Hickel, T.; Neugebauer, J.; Kresse, G.; Janotti, A.; Van de Walle, C. G. First-principles calculations for point defects in solids. *Rev. Mod. Phys.* **2014**, *86*, 253–305.
- (9) Oba, F.; Choi, M.; Togo, A.; Tanaka, I. Point defects in ZnO: an approach from first principles. *SCIENCE AND TECHNOLOGY OF ADVANCED MATERIALS* **2011**, *12*.
- (10) Pochet, P.; Caliste, D. Point defect diffusion in Si and SiGe revisited through atomistic simulations. *MATERIALS SCIENCE IN SEMICONDUCTOR PROCESSING* **2012**, *15*, 675–690.
- (11) Lany, S.; Zunger, A. Assessment of correction methods for the band-gap problem and for finite-size effects in supercell defect calculations: Case studies for ZnO and GaAs. *Phys. Rev. B* **2008**, *78*, 235104.
- (12) Freysoldt, C.; Neugebauer, J. First-principles calculations for charged defects at surfaces, interfaces, and two-dimensional materials in the presence of electric fields. *Phys. Rev. B* **2018**, *97*, 205425.

- (13) Frey, N. C.; Akinwande, D.; Jariwala, D.; Shenoy, V. B. Machine Learning-Enabled Design of Point Defects in 2D Materials for Quantum and Neuromorphic Information Processing. *ACS Nano* **2020**, *14*, 13406–13417.
- (14) Deml, A. M.; Holder, A. M.; O’Hayre, R. P.; Musgrave, C. B.; Stevanović, V. Intrinsic Material Properties Dictating Oxygen Vacancy Formation Energetics in Metal Oxides. *The Journal of Physical Chemistry Letters* **2015**, *6*, 1948–1953.
- (15) Wexler, R. B.; Gautam, G. S.; Stechel, E. B.; Carter, E. A. Factors Governing Oxygen Vacancy Formation in Oxide Perovskites. *Journal of the American Chemical Society* **2021**, *143*, 13212–13227.
- (16) Park, J.; Xu, B.; Pan, J.; Zhang, D.; Lany, S.; Liu, X.; Luo, J.; Qi, Y. Accurate prediction of oxygen vacancy concentration with disordered A-site cations in high-entropy perovskite oxides. *npj Computational Materials* **2023**, *9*.
- (17) Yan, Q.; Kar, S.; Chowdhury, S.; Bansil, A. The Case for a Defect Genome Initiative. *Advanced Materials* **2024**, *36*, 2303098.
- (18) Chen, C.; Ye, W.; Zuo, Y.; Zheng, C.; Ong, S. P. Graph Networks as a Universal Machine Learning Framework for Molecules and Crystals. *Chem. Mater.* **2019**, *31*, 3564–3572.
- (19) Reiser, P.; Neubert, M.; Eberhard, A.; Torresi, L.; Zhou, C.; Shao, C.; Metni, H.; van Hoesel, C.; Schopmans, H.; Sommer, T.; Friederich, P. Graph neural networks for materials science and chemistry. *Commun. Mater.* **2022**, *3*, 93.
- (20) Fung, V.; Zhang, J.; Juarez, E.; Sumpter, B. G. Benchmarking graph neural networks for materials chemistry. *npj Comput. Mater.* **2021**, *7*, 84.
- (21) Xie, T.; Grossman, J. C. Crystal Graph Convolutional Neural Networks for an Accurate and Interpretable Prediction of Material Properties. *Phys. Rev. Lett.* **2018**, *120*, 145301.

- (22) Kazeev, N.; Al-Maeni, A. R.; Romanov, I.; Faleev, M.; Lukin, R.; Tormasov, A.; Castro Neto, A. H.; Novoselov, K. S.; Huang, P.; Ustyuzhanin, A. Sparse representation for machine learning the properties of defects in 2D materials. *npj Computational Materials* **2023**, *9*.
- (23) Xiang, X.; Soh, D.; Dunham, S. Exploration of Deep Learning Models for Accelerated Defect Property Predictions and Device Design of Cubic Semiconductor Crystals. *The Journal of Physical Chemistry C* **2024**, *128*, 8821–8829.
- (24) Rahman, M. H.; Gollapalli, P.; Manganaris, P.; Yadav, S. K.; Pilania, G.; DeCost, B.; Choudhary, K.; Mannodi-Kanakkithodi, A. Accelerating defect predictions in semiconductors using graph neural networks. *APL Machine Learning* **2024**, *2*, 016122.
- (25) Li, Q.; Han, Z.; Wu, X.-m. Deeper Insights Into Graph Convolutional Networks for Semi-Supervised Learning. *Proceedings of the AAAI Conference on Artificial Intelligence* **2018**, *32*.
- (26) Pun, C. S.; Lee, S. X.; Xia, K. Persistent-homology-based machine learning: a survey and a comparative study. *Artif. Intell. Rev.* **2022**, *55*, 5169–5213.
- (27) Wu, K.; Zhao, Z.; Wang, R.; Wei, G.-W. TopP-S: Persistent homology-based multi-task deep neural networks for simultaneous predictions of partition coefficient and aqueous solubility. *Journal of Computational Chemistry* **2018**, *39*, 1444–1454.
- (28) Cang, Z.; Wei, G.-W. TopologyNet: Topology based deep convolutional and multi-task neural networks for biomolecular property predictions. *PLOS Computational Biology* **2017**, *13*, 1–27.
- (29) Jiang, Y.; Chen, D.; Chen, X.; Li, T.; Wei, G.-W.; Pan, F. Topological representations of crystalline compounds for the machine-learning prediction of materials properties. *npj Computational Materials* **2021**, *7*.

- (30) Fang, Z.; Yan, Q. Towards accurate prediction of configurational disorder properties in materials using graph neural networks. *npj Computational Materials* **2024**, *10*.
- (31) Roedel, J.; Jo, W.; Seifert, K. T. P.; Anton, E.-M.; Granzow, T.; Damjanovic, D. Perspective on the Development of Lead-free Piezoceramics. *JOURNAL OF THE AMERICAN CERAMIC SOCIETY* **2009**, *92*, 1153–1177.
- (32) Dey, T. K.; Wang, Y. *Computational topology for data analysis*; Cambridge University Press, 2022.
- (33) Aktas, M. E.; Akbas, E.; El Fatmaoui, A. Persistence homology of networks: methods and applications. *APPLIED NETWORK SCIENCE* **2019**, *4*.
- (34) Zia, A.; Khamis, A.; Nichols, J.; Tayab, U. B.; Hayder, Z.; Rolland, V.; Stone, E.; Petersson, L. Topological deep learning: a review of an emerging paradigm. *ARTIFICIAL INTELLIGENCE REVIEW* **2024**, *57*.
- (35) Jain, A.; Ong, S. P.; Hautier, G.; Chen, W.; Richards, W. D.; Dacek, S.; Cholia, S.; Gunter, D.; Skinner, D.; Ceder, G.; Persson, K. A. Commentary: The Materials Project: A materials genome approach to accelerating materials innovation. *APL Materials* **2013**, *1*, 011002.
- (36) Morris, C.; Ritzert, M.; Fey, M.; Hamilton, W. L.; Lenssen, J. E.; Rattan, G.; Grohe, M. Weisfeiler and Leman Go Neural: Higher-Order Graph Neural Networks. *Proceedings of the AAAI Conference on Artificial Intelligence* **2019**, *33*, 4602–4609.
- (37) Reiser, P.; Neubert, M.; Eberhard, A.; Torresi, L.; Zhou, C.; Shao, C.; Metni, H.; van Hoesel, C.; Schopmans, H.; Sommer, T.; Friederich, P. Graph neural networks for materials science and chemistry. *COMMUNICATIONS MATERIALS* **2022**, *3*.
- (38) Veličković, P.; Cucurull, G.; Casanova, A.; Romero, A.; Liò, P.; Bengio, Y. Graph Attention Networks. International Conference on Learning Representations. 2018.

- (39) Brody, S.; Alon, U.; Yahav, E. How Attentive are Graph Attention Networks? International Conference on Learning Representations. 2022.
- (40) Shi, Y.; Huang, Z.; Feng, S.; Zhong, H.; Wang, W.; Sun, Y. Masked Label Prediction: Unified Message Passing Model for Semi-Supervised Classification. Proceedings of the Thirtieth International Joint Conference on Artificial Intelligence, IJCAI-21. 2021; pp 1548–1554.
- (41) Alkauskas, A.; Yan, Q.; Van de Walle, C. G. First-principles theory of nonradiative carrier capture via multiphonon emission. *Phys. Rev. B* **2014**, *90*, 075202.
- (42) Freysoldt, C.; Neugebauer, J.; Van de Walle, C. G. Fully Ab Initio Finite-Size Corrections for Charged-Defect Supercell Calculations. *Phys. Rev. Lett.* **2009**, *102*, 016402.
- (43) Das, T.; Nicholas, J. D.; Qi, Y. Polaron size and shape effects on oxygen vacancy interactions in lanthanum strontium ferrite. *Journal of materials chemistry. A, Materials for energy and sustainability* **2017**, *5*, 25031–25043.
- (44) Park, J.; Xu, B.; Pan, J.; Zhang, D.; Lany, S.; Liu, X.; Luo, J.; Qi, Y. Accurate prediction of oxygen vacancy concentration with disordered A-site cations in high-entropy perovskite oxides. *npj computational materials* **2023**, *9*, 29–13.
- (45) Greenacre, M.; Groenen, P. J. F.; Hastie, T.; D’Enza, A. I.; Markos, A.; Tuzhilina, E. Publisher Correction: Principal component analysis. *Nature Reviews Methods Primers* **2023**, *3*.
- (46) Wan, Z.; Wang, Q.-D.; Liu, D.; Liang, J. Data-driven machine learning model for the prediction of oxygen vacancy formation energy of metal oxide materials. *Physical chemistry chemical physics : PCCP* **2021**, *23*, 15675–15684.
- (47) Park, S.; Lee, N.; Park, J. O.; Park, J.; Heo, Y. S.; Lee, J. Exploring the Latent Chemical

- Space of Oxygen Vacancy Formation Energy by a Machine Learning Ensemble. *ACS Materials Letters* **2024**, *6*, 66–72.
- (48) Baldassarri, B.; He, J.; Gopakumar, A.; Griesemer, S.; Salgado-Casanova, A. J. A.; Liu, T.-C.; Torrisi, S. B.; Wolverton, C. Oxygen Vacancy Formation Energy in Metal Oxides: High-Throughput Computational Studies and Machine-Learning Predictions. *Chemistry of Materials* **2023**, *35*, 10619–10634.
- (49) Kresse, G.; Hafner, J. Ab initio molecular dynamics for liquid metals. *Phys. Rev. B* **1993**, *47*, 558–561.
- (50) Kresse, G.; Furthmüller, J. Efficiency of ab-initio total energy calculations for metals and semiconductors using a plane-wave basis set. *Comput. Mater. Sci.* **1996**, *6*, 15–50.
- (51) Kresse, G.; Joubert, D. From ultrasoft pseudopotentials to the projector augmented-wave method. *Phys. Rev. B* **1999**, *59*, 1758–1775.
- (52) Blöchl, P. E. Projector augmented-wave method. *Phys. Rev. B* **1994**, *50*, 17953–17979.
- (53) Perdew, J. P.; Burke, K.; Ernzerhof, M. Generalized Gradient Approximation Made Simple. *Phys. Rev. Lett.* **1996**, *77*, 3865–3868.
- (54) Grimme, S.; Antony, J.; Ehrlich, S.; Krieg, H. A consistent and accurate ab initio parametrization of density functional dispersion correction (DFT-D) for the 94 elements H-Pu. *The Journal of chemical physics* **2010**, *132*, 154104–154104–19.
- (55) Grimme, S.; Ehrlich, S.; Goerigk, L. Effect of the damping function in dispersion corrected density functional theory. *Journal of computational chemistry* **2011**, *32*, 1456–1465.
- (56) Akiba, T.; Sano, S.; Yanase, T.; Ohta, T.; Koyama, M. Optuna: A Next-Generation Hyperparameter Optimization Framework. Proceedings of the 25th ACM SIGKDD International Conference on Knowledge Discovery & Data Mining. 2019; p 2623–2631.

- (57) Bergstra, J.; Bardenet, R.; Bengio, Y.; Kégl, B. Algorithms for Hyper-Parameter Optimization. *Advances in Neural Information Processing Systems*. 2011.

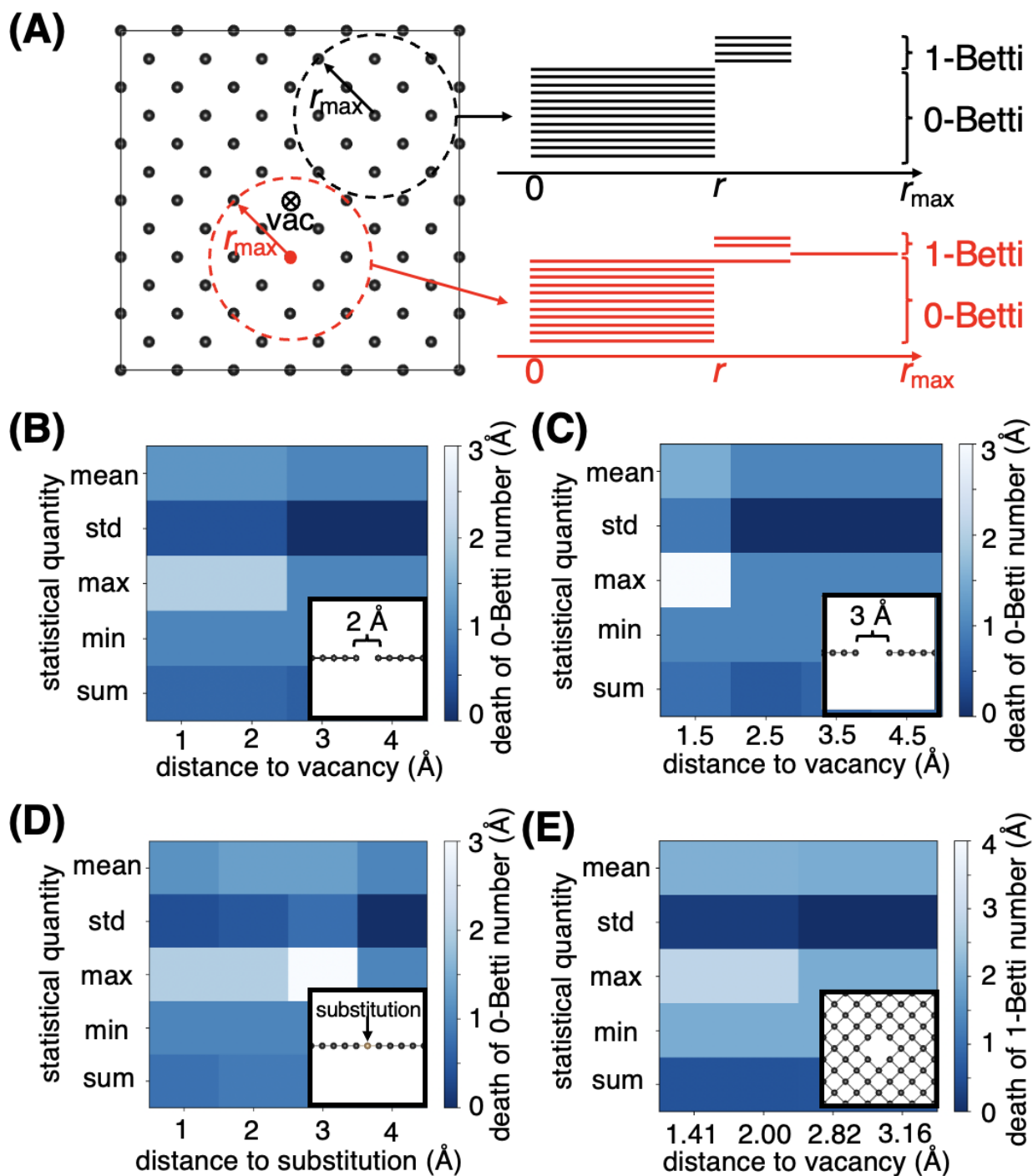


Figure 1: (A) A schematic plot of the procedure to calculate atoms-specific persistent homology features for a two-dimensional lattice. (B) The calculated statistical quantity of the death of 0-Betti number features for the one-dimensional toy model with one vacancy. (C, D) Same as (B), but for the toy model with two adjacent vacancies and with a substitution defect respectively. (E) The calculated statistical quantity of the death of the 1-Betti number features for the two-dimensional toy model with one vacancy.

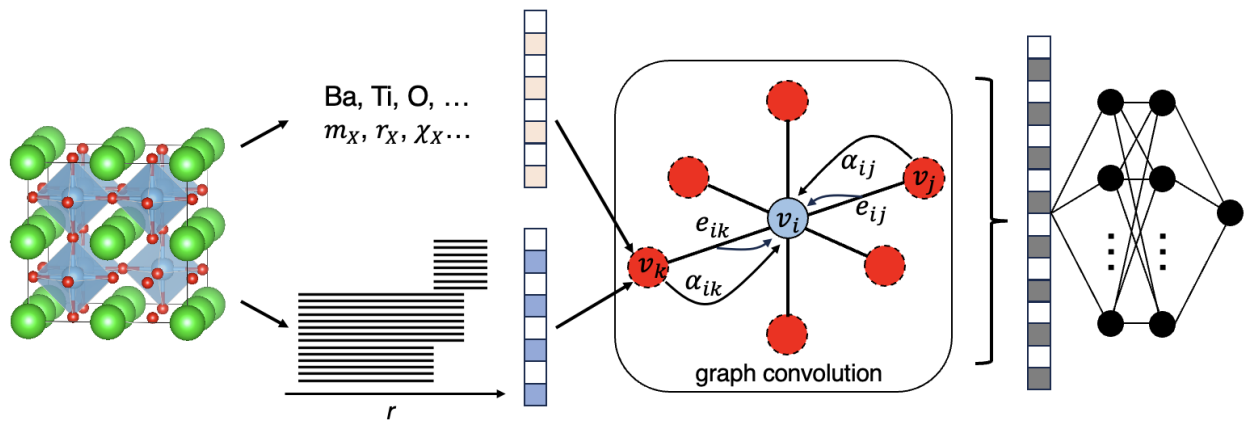


Figure 2: A schematic plot of the GNN model based on the attention mechanism to predict the defect formation energies. The input defective structure will be converted into the crystal graph, where node features contain both the elemental attributes (such as the mass m_X , the radius r_X , and the electronegativity χ_X of element X) and the ASPH features. The graph passes through several graph convolution layers, where features on adjacent nodes exchange and aggregate. The convoluted node features will be gathered together into a global latent representation of the graph and pass through a multi-perceptron network to predict the defect formation energy.

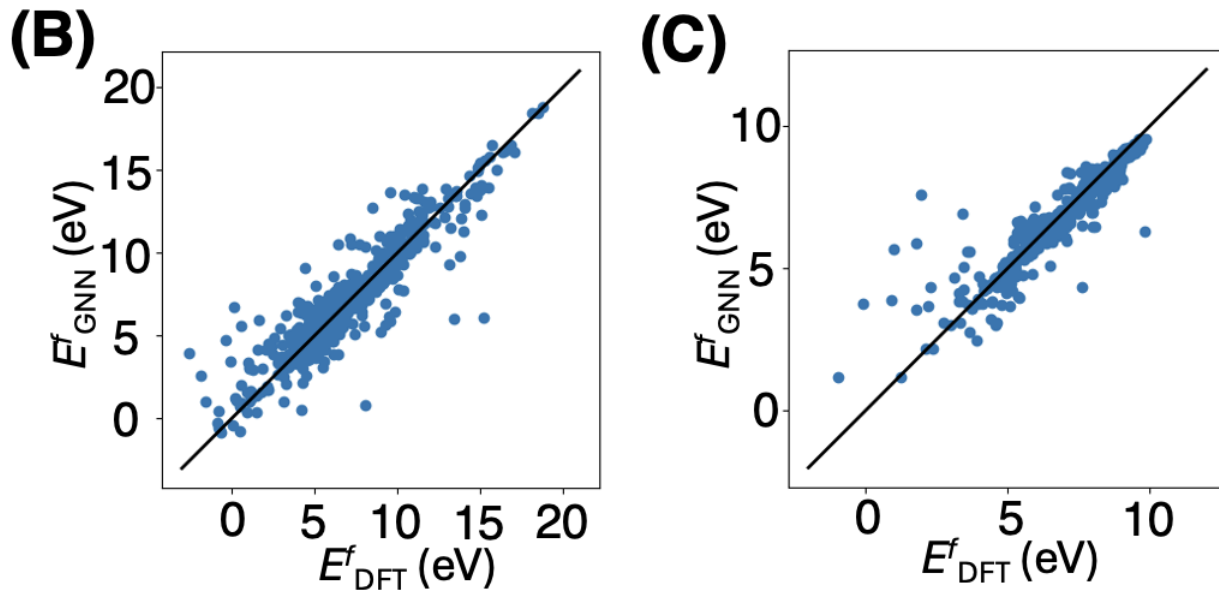
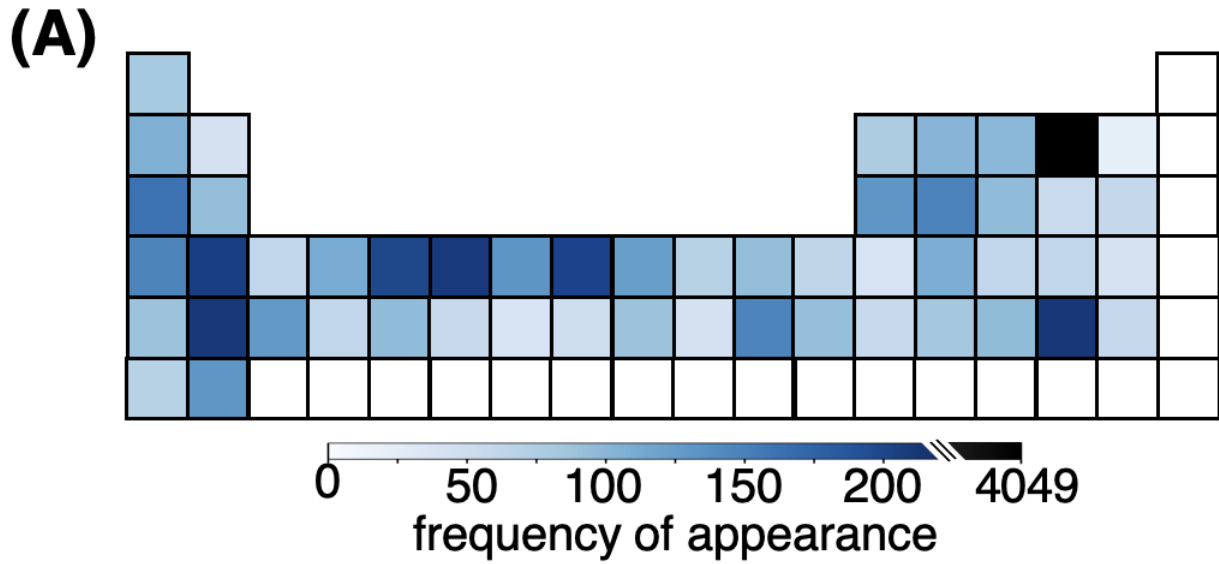


Figure 3: (A) The number of vacancies of each elemental type in our constructed O-based perovskite dataset. Vacancies of all elements before La, except for noble gas elements, are present in our dataset. (B) The comparison between vacancy formation energies obtained from DFT methods and from GNN predictions on the testing set of the dataset. (C) Same as (B), but for the dataset with only O vacancies.

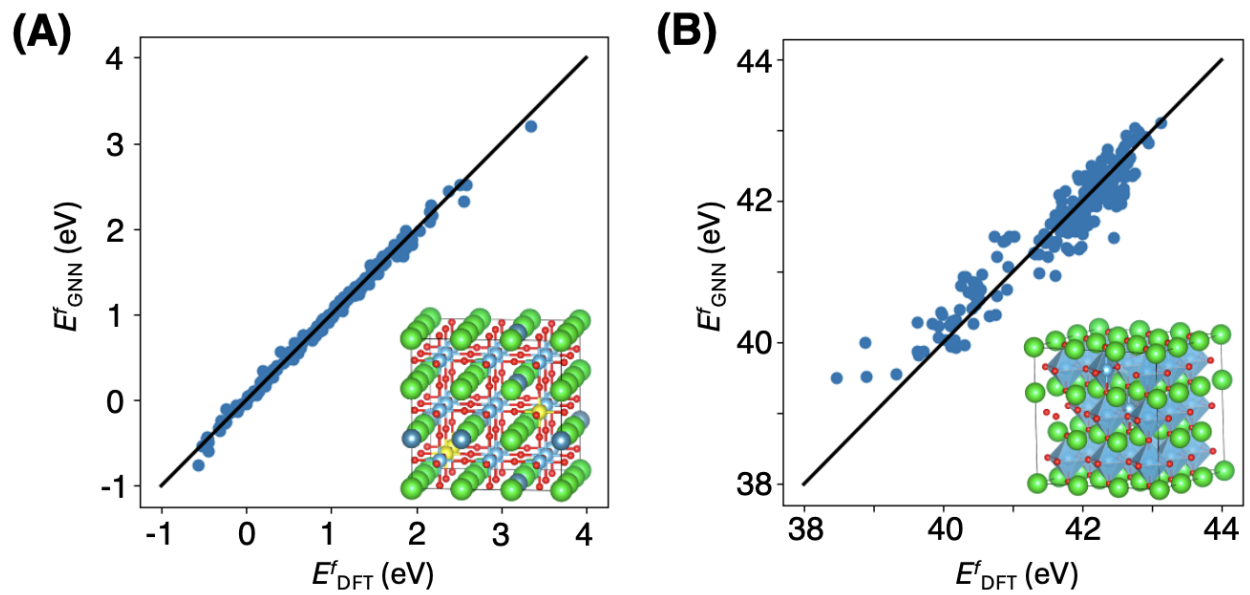


Figure 4: (A) The comparison between the defect formation energies from the DFT method and the GNN model on the testing set of the BaTiO₃ dataset with multiple substitutions. The inset is a typical structure in the dataset, with the following color code: light green: Ba; dark green: Sr; grey: Ca; yellow: Zr; cyan: Ti; red: O. (B) Same as (A), but for the dataset of BaTiO₃ with multiple vacancies.